Multi-omic profiling to assess the effect of iron starvation in *Streptococcus pneumoniae* TIGR4

Irene Jiménez-Munguía[1], Mónica Calderón-Santiago[2], Antonio Rodríguez-Franco[1], Feliciano Priego-Capote[2] and Manuel J. Rodríguez-Ortega[1]

[1] Departamento de Bioquímica y Biología Molecular, Universidad de Córdoba; Campus de Excelencia Internacional CeiA3, Córdoba, Spain

[2] Departamento de Química Analítica, Universidad de Córdoba; Campus de Excelencia Internacional CeiA3, Córdoba, Spain

ABSTRACT

We applied multi-omics approaches (transcriptomics, proteomics and metabolomics) to study the effect of iron starvation on the Gram-positive human pathogen *Streptococcus pneumoniae* to elucidate global changes in the bacterium in a condition similar to what can be found in the host during an infectious episode. We treated the reference strain TIGR4 with the iron chelator deferoxamine mesylate. DNA microarrays revealed changes in the expression of operons involved in multiple biological processes, with a prevalence of genes coding for ion binding proteins. We also studied the changes in protein abundance by 2-DE followed by MALDI-TOF/TOF analysis of total cell extracts and secretome fractions. The main proteomic changes were found in proteins related to the primary and amino sugar metabolism, especially in enzymes with divalent cations as cofactors. Finally, the metabolomic analysis of intracellular metabolites showed altered levels of amino sugars involved in the cell wall peptidoglycan metabolism. This work shows the utility of multi-perspective studies that can provide complementary results for the comprehension of how a given condition can influence global physiological changes in microorganisms.

Submitted 28 February 2018
Accepted 23 May 2018
Published 13 June 2018

Corresponding author
Manuel J. Rodríguez-Ortega, mjrodriguez@uco.es

Academic editor
Luciana Leite

Additional Information and Declarations can be found on page 17

DOI **10.7717/peerj.4966**

Subjects Biochemistry, Microbiology, Data Science
Keywords Transcriptomics, Proteomics, Metabolomics, Iron deprivation, Pneumococcus, Omics

INTRODUCTION

Bacteria need a plethora of factors for optimal growth, with iron being an essential micronutrient. Within the human body, the free concentration of this element is approximately 10^{-18} M (*Yang et al., 2014*), which is too low to hold a growth capable of supporting bacterial infections. The low concentrations of free iron within the host are due to the scavenging of this element by different high-affinity proteins (e.g., transferrin, lactoferrin, haemoglobin, etc.) (*Froehlich, Bates & Scott, 2009*). Therefore, in order to survive in the host, pathogens need to develop special strategies to uptake the minimum amount that they require of such a nutrient (*Nanduri et al., 2008*), such as the direct extraction of this metal cation from host iron-containing proteins, or by capturing ferric-binding siderophores from host environments via ABC transporters (*Ge & Sun, 2014*).

Moreover, the capacity of bacterial pathogens for iron acquisition itself represents an important virulence determinant (*Kanaujia et al., 2015*). In addition, pathogens can also modify their energetic metabolism to adapt to the environmental situation within the host.

Streptococcus pneumoniae, also known as the pneumococcus, is a Gram-positive microorganism that lives as a commensal in the human respiratory tract and that, under appropriate circumstances, becomes pathogenic, being able to cause high morbidity and mortality (*Blasi et al., 2012*; *Olaya-Abril et al., 2014b*). This bacterium is a major cause of mucosal diseases such as otitis media and sinusitis, and is a prevalent pathogen in different invasive diseases including pneumonia, bacteremia, meningitis, and sepsis (*O'Brien et al., 2009*). Pneumococcal pneumonia, which is the major clinical manifestation of pneumococcal infections, affects mainly young children and the elderly although all age groups may be affected. It has been estimated that almost one million children die every year because of pneumococcal diseases, with >90% of these deaths occurring in developing countries (*Johnson et al., 2010*). Pneumococcal infections also represent a high burden of disease in adults of developed countries. Actually, around 25,000 deaths are registered every year in the United States in adults >50 years of age, and in European countries the pneumococcus also causes significant mortality and morbidity (*Olaya-Abril et al., 2013*; *Weycker et al., 2010*). Therefore, understanding the basics of host-pathogen interactions is critical to effectively fight against infections.

In the context of systems biology, the use of massive analysis platforms is highly valuable to understand biological processes (*Fondi & Lio, 2015*; *Kohlstedt et al., 2014*). However, single-omic datasets, although powerful, offer a partial view of a biological system (*Grady et al., 2017*). Studying the responses of any biological system to a given condition using transcriptomics, proteomics and/or metabolomics can greatly help to elucidate the global adaptation to such a condition, i.e., stress, pathological status, nutrient availability/limitation, etc (*Dall'Agnol et al., 2014*; *Feng et al., 2011*; *Fu et al., 2013*; *Yang et al., 2012*). To this regard, we have approached from the in vitro bacterial culture to what it should actually occur in vivo, mimicking the iron restriction in order to describe the global changes that the pneumococcus undergoes and, therefore, to understand mechanisms of adaptation when it infects the host. To this end, we have studied the responses of the reference pneumococcal strain TIGR4 in an iron-deprived medium, at three different –omic levels: transcriptomics, proteomics and metabolomics. We have identified sets of genes, proteins and metabolites that are differentially expressed/synthesized under the studied nutrient restriction.

MATERIALS AND METHODS

Bacterial strains and culture conditions

S. pneumoniae TIGR4 was grown without agitation at 37 °C in air with 5% CO_2 in Todd Hewitt Broth (THB) until mid-exponential phase (OD_{600} = 0.3), and kept at −80 °C with 20% glycerol. Three different biological replicates were made for proteomics and metabolomics experiments, and four replicates for transcriptomics (20 mL, 100 mL, and 200 mL cultures to perform transcriptomics, metabolomics, and proteomics experiments,

respectively). Each set of replicates was standardised by inoculum, using starter cultures from glycerol-kept vials, in order to prepare the standard inoculum that was further added to the different biological replicates for each "ome" extraction. Iron-depleted cultures were prepared by adding deferoxamine (DFO) mesylate salt (Sigma) dissolved in water, at 100 μM, according to the dose used for this chelator in other works for the pneumococcus (*Trappetti et al., 2011*).

Protein extracts

Total cellular proteins and secreted proteins were obtained as described (*Mitsuwan et al., 2017*). Briefly, to obtain cellular proteins, pellets were washed three times in sterile phosphate buffered saline (PBS) pH 7.4. Bacterial cell wall was digested at 37 °C with top-down agitation by adding 100 U mutanolysin (Sigma–Aldrich, St. Louis, MO, USA). Protoplasts were resuspended in 4 mL of rehydration buffer (7 M urea, 2 M thiourea, 4% CHAPS, 0.5% Triton X-100, 0.005% bromophenol blue, 0.5% Bio-lyte 3–10 ampholytes (Bio-Rad, Hercules, CA, USA)) and disrupted by sonication (6 cycles; 20-s pulses, 90% amplitude). Proteins were recovered by centrifugation (5,000× g, 7 min), dialyzed and concentrated using a centrifugal filter device (Amicon Ultra15, 10 kDa; Millipore, Burlington, MA, USA). To obtain secretome fractions, proteins were precipitated from the supernatants with 10% trichloroacetic acid, after removing cell debris through filter devices (0.22 μm, Millipore, Burlington, MA, USA). Protein pellets were washed twice with 1 mL of ice-cold absolute ethanol. Finally, proteins were air-dried and resuspended in 500 μL of rehydration buffer.

Two-dimensional polyacrylamide gel electrophoresis and image analysis

Protein samples were cleaned using the 2-D clean up kit (Life Sciences, Marlborough, MA, USA) according to manufacturer's instructions. Proteins were resuspended in 200 μL of rehydration buffer and quantified by the Bradford method (*Bradford, 1976*). Five hundred μg of protein were subjected to isoelectric focusing (IEF) on 18 cm Immobiline DryStrips immobilized pH gradient (IPG) gel strips (4–7 pH linear gradient (Life Sciences, Marlborough, MA, USA)). The strips were loaded onto a Bio-Rad Protean IEF Cell system (Bio Rad, Hercules, CA, USA), and IEF was performed at 20 °C using the following conditions: 2 h of passive rehydration, 50 V for 10 h followed by a voltage-ramp (250 V for 15 min; 500 V for 30 min; 1,000 V for 1 h; 2,000 V for 1 h; 5,000 V for 1 h; 8,000 V for 2 h); finally, proteins were focused on 70,000 Vh. Before the second dimension, the IPG strips were first soaked for 15 min in equilibration solution (50 mM Tris- HCl buffer, pH 8.8, 6 M urea, 30% v/v glycerol, 2% SDS, and bromophenol blue traces) containing 2.5 mg/mL DTT, and subsequently soaked for 15 min in equilibration solution containing 45 mg/mL iodoacetamide. The second dimension was performed on 12% polyacrylamide gels, using the Protean plus Dodeca Cell system (Bio-Rad, Hercules, CA, USA). Gels were run at 90 V until the dye reached the bottom. Then, gels were stained with brilliant blue G-colloidal solution (Sigma-Aldrich, St. Louis, MO, USA) according to manufacturer's instructions. Gels were scanned with a GS-800 densitometer (Bio-Rad, Hercules, CA, USA). Digitized

images were analyzed with PD-Quest v8.1.0 (Bio-Rad, Hercules, CA, USA). Two analytical gels were made per sample (i.e., biological replicate and protein extraction). Consistent spots were considered as those whose presence remained constant at the three biological replicates. Spots showing a consistent change in the intensity value of at least twofold were included in the quantitative analysis.

Protein identification by MALDI-TOF/TOF MS/MS

Spots excision, protein digestion, peptide desalting and mass spectrometry analysis were performed as already described by our group (*Mitsuwan et al., 2017*) with slight modifications: after mass spectra acquisition using a MALDI-TOF/TOF (4800 Proteomics Analyzer, Applied Biosystems, Foster City, CA, USA) mass spectrometer in the m/z range 800 to 4,000, Mascot 2.0 search engine (Matrix Science Ltd., London, UK) was used for protein identification running on GPS Explorer^{TM} software v3.5 (Applied Biosystems, Foster City, CA, USA) over the National Center for Biotechnology Information (NCBI) protein database (updated monthly). Search setting allowed one missed cleavage with the selected trypsin enzyme, *Streptococcus pneumoniae* for taxonomy restrictions, cysteine carbamidomethylation as a fixed modification, methionine oxidation as a variable modification, a MS/MS fragment tolerance of 0.2 Da, and a precursor mass tolerance of 10 ppm. Identifications with a Mascot score >70 (p-value <0.05) were considered as significant.

Inductively coupled plasma-mass spectrometry (ICP-MS) analysis

Iron concentration in THB medium was determined by ICP-MS. Five ml aliquots of samples were chemically digested with 2 mL concentrated nitric acid on a hot plate with a heating ramp of 20 °C until reaching 130 °C, maintaining this temperature for 2 hours. High purity deionized water was added to the digested samples to a final volume of 25 mL. Rh-solution was added as internal standard (final concentration of 10 μg/L). The isotope ^{56}Fe and the internal standard were analyzed with a NexION 350X instrument (PerkinElmer, Waltham, MA, USA), equipped with a PFA concentric microFlow nebulizer and a cyclonic PFA spray chamber, and operated at 1,600 W in He collision mode. Results were expressed as μg of Fe per liter of culture.

RNA isolation

Cells resuspended in 1 mL of Tri-Reagent (Sigma–Aldrich, St. Louis, MO, USA) were disrupted by vortexing (20 min) with 0.5 g of glass beads (Sigma–Aldrich, St. Louis, MO, USA). After recovering the supernatant by centrifugation (1 min, 12,000× g, 4 °C), 200 μL of chloroform were added. Samples were centrifuged again (12,000× g for 15 min; 4 °C) and 500 μL of ice-cold isopropanol were added. After 15 min incubation (4 °C), samples were centrifuged (30 min, 12,000× g, 4 °C) and washed with 500 μL of 70% ice-cold ethanol. RNA was air-dried and resuspended in 40 μL of distilled water previously treated with 1% of diethylpyrocarbonate (DEPC). Samples were treated with DNAse (Ambion, Austin, TX, USA) according to manufacturer's instructions.

RNA amplification, labeling and hybridization to DNA microarrays

RNA quality was assessed using a TapeStation (Agilent Technologies, Santa Clara, CA, USA). The RNA integrity number (RIN) ranged between 7.0 and 9.2. Samples with RIN >7 were considered for analysis. RNA concentration and dye incorporation were measured using a UV–VIS spectrophotometer (Nanodrop 1000, Agilent Technologies, Santa Clara, CA, USA). Hybridization to custom 8 × 15 K Gene Expression Microarrays (ID 044371, Agilent Technologies, Santa Clara, CA, USA) containing the whole genome of *S. pneumoniae* TIGR4 was conducted following manufacturer's protocol using a two-color (Cy3 and Cy5) Microarray-Based Gene Expression Analysis (v. 6.5, Agilent Technologies, Santa Clara, CA, USA). Microarrays were then washed and scanned using a DNA Microarray Scanner (Model G2505C).

Gene expression analysis

Microarray hybridization data were obtained with the Feature Extraction Software v. 10.7 (Agilent Technologies, Santa Clara, CA, USA), using the default variables. Data analysis was performed using the R Limma *Bioconductor* package (*Ritchie et al., 2015*), according to a direct two color design. A total of eight microarrays were done, corresponding to four biological replicates for each condition using swapped and random mixtures to cope with batch effects. Functional annotation of the differentially expressed genes was done using embedded BlastX included into the *Blast2GO* program (*Conesa et al., 2005*) using the public NCBI nr database. Raw feature intensities were corrected using the *Normexp* background correction algorithm. An initial within-array normalization was done using spatial and intensity-dependent *Loess* method, followed by a between-array *Aquantile* normalization. Normalized data are shown in Figs. S1 and S2. Differential expression was ordered according to their adjusted *p*-values, and the expression of each gene is reported as the log_2 ratio of the value obtained for each condition compared to control condition. A gene was considered differentially expressed if it displayed an adjusted *p*-value less than 0.05 by the Student *t*-test. Finally, over- and under- expressed genes were analyzed in terms of gene ontology by using a hypergeometric analysis (GOStats package). Prediction of operons was obtained from the DOOR database (*Dam et al., 2007*; *Mao et al., 2009*).

Preparation of intracellular metabolite samples

Cell pellets were washed twice with PBS and resuspended in lysis buffer (PBS and 30% sucrose) containing 100 U mutanolysin. Samples were incubated at 37 °C overnight. Metabolic quenching was achieved by adding ice-cold 50% methanol. Cells were disrupted by sonication (6 cycles: 20 s, 90% amplitude). After centrifugation (5,000× g, 7 min), cell debris was separated through 0.22 μm membrane filters (Millipore, Burlington, MA, USA). Then, supernatants were collected and ultracentrifuged (100,000× g; 1.5 h, 4 °C). Finally, metabolite samples were kept at −80 °C before analysis.

Analysis of intracellular metabolites

Intracellular metabolite samples were analyzed by LC–QTOF MS/MS using an Agilent 1200 Series LC system coupled to an Agilent 6540 UHD Accurate-Mass QTOF hybrid mass spectrometer equipped with dual electrospray (ESI) source as described (*Mitsuwan*

et al., 2017) without modifications. Briefly, chromatography was performed using a C18 reverse-phase analytical column (Mediterranean, 50 mm × 0.46 mm *i.d.,* 3 μm particle size; Teknokroma, Barcelona, Spain), thermostated at 25 °C. The mobile phases were 5% ACN (phase A) and 95% ACN (phase B) both with 0.1% formic acid as ionization agent. The LC pump was programmed with a flow rate of 0.8 mL/min with the following elution gradient: 3% phase B was kept as initial mobile phase constant from min 0 to 1; from 3 to 100% of phase B from min 1 to 13. A post-time of 5 min was set to equilibrate the initial conditions for the next analysis. The injection volume was 3 μL and the injector needle was washed for 10 times between injections with 80% methanol. The parameters of the electrospray ionization source, operating in negative and positive ionization mode, were as follows: the capillary and fragmentor voltage were set at ±3.5 kV and 175 V, respectively; N_2 in the nebulizer was flowed at 40 psi; the flow rate and temperature of the N_2 as drying gas were 8 L/min and 350 °C, respectively. MS and MS/MS data were collected in both polarities using the centroid mode at a rate of 2.6 spectra per second in the extended dynamic range mode (2 GHz). Accurate mass spectra in auto MS/MS mode were acquired in bot MS and MS/MS m/z ranges of 60–1,100 Da. To assure the desired mass accuracy of recorded ions, continuous internal calibration was performed during analyses by using the signals at m/z 121.0509 (protonated purine) and m/z 922.0098 (protonated hexakis (1H, 1H, 3H-tetrafluoropropoxy) phosphazine or HP-921) in positive ion mode; while in negative ion mode ions with m/z 119.0362 (proton abstracted purine) and m/z 966.0007 (formate adduct of HP-921) were used. The auto MS/MS mode was configured with two maximum precursors per cycle and an exclusion window of 0.25 min after two consecutive selections of the same precursor. The collision energy selected was 20 V.

Metabolomics data processing and identification

MassHunter Workstation software (version 5.00 Qualitative Analysis, Agilent Technologies, Santa Clara, CA, USA) was used to process all data obtained by LC–QTOF in auto MS/MS mode. Treatment of raw data files was initiated by extraction of potential molecular features (MFs) with the suited algorithm included in the software. For this purpose, the extraction algorithm considered all ions exceeding 1,000 counts with a single charge state. Additionally, the isotopic distribution to consider a molecular feature as valid should be defined by two or more ions (with a peak spacing tolerance of 0.0025 *m/* z, plus 10.0 ppm in mass accuracy). Adduct formation in the positive (+Na) and negative (+HCOO) modes, as well as neutral loss by dehydration were included to identify features corresponding to the same potential metabolite. Then, MFs, characterized by their retention time, intensity in the apex of chromatographic peak and accurate mass, were exported in compound exchange format files (.cef files) and imported into Mass Profiler Professional (MPP) software package (version 12.1, Agilent Technologies, Santa Clara, CA, USA) for alignment and further processing. MPP allowed statistical analysis by Volcano plot (a combination of analysis of variance and fold change analysis). The MS/MS METLIN Personal Compound and Database Library (PCDL) was used to identify significant compounds using both MS and MS/MS information to assure metabolite identification. To identify compounds with

no MS/MS information in the METLIN Database, MetaCyc database, and the MassBank database were used.

Statistical analysis

All the quantitative analyses (transcriptomics, proteomics, and metabolomics) were performed from three or four independent biological replicates, and the results are expressed as the mean ± standard deviation. Paired data were analyzed by univariate analysis using the Student's *t*-test. Principal component analysis (PCA) was done with the web-based software NIA array analysis tool (http://lgsun.grc.nia.nih.gov/anova/index.html) (*Sharov, Dudekula & Ko, 2005*). *p*-Values lower than 0.05 were considered statistically significant.

RESULTS

Effect of iron starvation on pneumococcal growth *in vitro*

S. pneumoniae TIGR4 was grown in THB, in which the iron concentration available for the bacteria, measured by ICP-MS, was 734 μg/L. In order to perform the further transcriptomic, proteomic and metabolomic analyses, we firstly monitored the growth of this strain in the presence of 100 μM DFO. As observed for other microorganisms, iron depletion caused a slight lag phase in the growth of pneumococcus (control growth rate: 1.93 h^{-1}; DFO-treated culture growth rate: 1.39 h^{-1}), and instead lead to a decrease in the OD at the plateau phase (Fig. 1). We chose the mid-exponential phase for sampling RNA, proteins and metabolites in curve points such that almost no delays in the time points of collecting cultures took place. These corresponded to OD = 0.3.

Transcriptomics

Limma analysis of the signals obtained after hybridizing the RNAs with the arrays revealed a number of differentially expressed genes when comparing the DFO treatment with its control (Supplemental Information 1): 338 genes changed significantly after DFO exposure, of which 118 genes increased their expression and 220 were down-regulated. Figure S3 shows the differentially expressed genes as a Volcano plot.

The $\log_2$ fold change values, resulting from averaging four independent biological replicates for each condition, ranged between 1.78 and −2.13. We noticed a consistent differential expression in which all of the genes pertaining to a same operon (according to the DOOR annotation database) changed in the same trend and even experienced almost identical $\log_2$ fold change values. We grouped the genes into operons according to the DOOR database (Supplemental Information 1). In total, 29 operons were clearly up-regulated, including those coding for the iron-compound ABC transporter system (genes SP_1869, SP_1870 and SP_1871), the closely neighbour gene SP_1872 coding for the iron-compound ABC transporter, the manganese ABC transporter system (genes SP_1648, SP_1649 and SP_1650), the ATP synthase complex (genes SP_1509 to SP_1513), and others including several transporter systems. Also, an operon containing genes for the riboflavin biosynthetic system (genes SP_0175 to SP_0178) was clearly up-regulated. Forty-four operons were clearly down-regulated, including the branched-chain amino

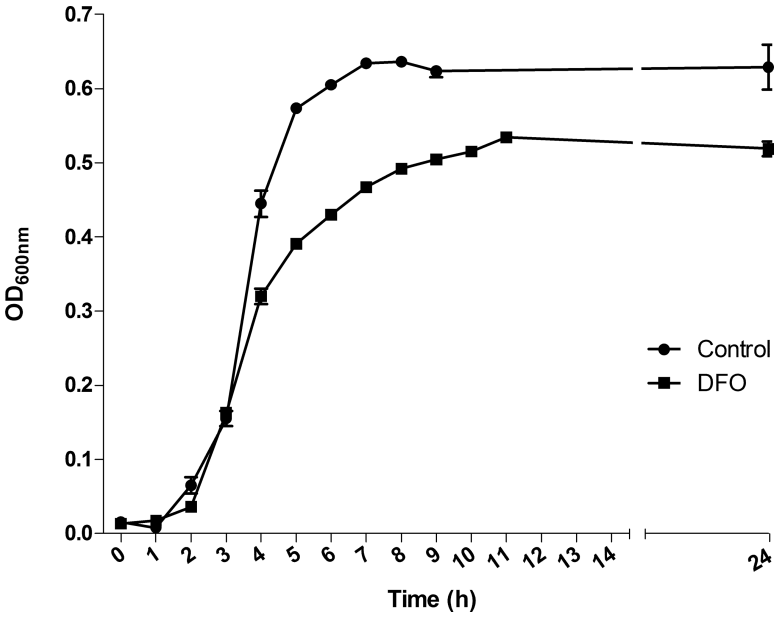

Figure 1 Effect of deferoxamine (DFO) on the growth of *Streptococcus pneumoniae* TIGR4. Each determination represents the mean of three different biological replicates. Solid circles indicate the mean ± standard deviation (SD) of untreated cultures; solid squares indicate the mean ± SD of DFO-treated cultures.

Full-size DOI: 10.7717/peerj.4966/fig-1

acid transporter system (genes SP_0750 to SP_0753) and the large operon of 13 genes (SP_0419 to SP_0431) involved in fatty acid biosynthesis, as well as two operons involved in competence (genes SP_0042 and SP_0043, and genes SP_2235 and SP_2236). In all the cases, the $\log_2$ FC values were almost identical for all the genes of the same operon. Table 1 shows the main operons that were differentially regulated.

The differentially expressed genes were annotated with Gene Ontology terms, using Blast2GO (Fig. 2). According to the molecular function level, the most enriched term among the over-expressed genes corresponded to "ion binding" (GO:0043167), representing around 25% of the genes. At the biological process level, the most enriched term was "cell metabolic process" (GO:0044237). For down-expressed genes, the most prevalent term at the biological process level was the same as for over-expressed genes, i.e., "cell metabolic process", and at the molecular function level, three different terms, including also that of "ion binding" (GO:0043167), represented around 13% each.

We validated the results obtained in the microarrays with RT-q-PCR on a subset of 16 differentially expressed genes of the TIGR4 strain (Table S1). For all the genes, there was the same trend (either over- or down-expression) and a high correlation ($r^2 = 0.93$) in the fold changes measured both at the microarray and the RT-q-PCR, thus confirming that the microarray data were reliable.

Proteomics

We compared the proteomes of two different protein fractions, cell extracts and secreted proteins, by 2-DE under iron deprivation conditions (Fig. S4). We then analyzed both the

Table 1 Operon distribution of differentially expressed genes under iron starvation.

ID Operon	Locus	Expressed genes	Change
38501	SP_0175, SP_0176, SP_0177, SP_0178	4/4	Upregulated
38508	SP_0202, SP_0203	2/2	Upregulated
38509	SP_0204, SP_0205, SP_0206, SP_0207	4/4	Upregulated
38541	SP_0385, SP_0386	2/3	Upregulated
38567	SP_0515, SP_0516	2/2	Upregulated
38588	SP_0599, SP_0600, SP_0601	3/4	Upregulated
38589	SP_0603, SP_0604	2/2	Upregulated
38594	SP_0622, SP_0623, SP_0624	3/4	Upregulated
38595	SP_0627, SP_0628	2/3	Upregulated
38600	SP_0661, SP_0662	2/2	Upregulated
38642	SP_0868, SP_0869	2/5	Upregulated
38672	SP_0999, SP_1000	2/2	Upregulated
38738	SP_1340, SP_1341, SP_1342, SP_1343, SP_1344	5/5	Upregulated
38776	SP_1509, SP_1510, SP_1511, SP_1512, SP_1513	5/8	Upregulated
38789	SP_1566, SP_1569	2/6	Upregulated
38795	SP_1591, SP_1592	2/2	Upregulated
38805	SP_1648, SP_1649, SP_1650	3/3	Upregulated
38808	SP_1662, SP_1665	2/8	Upregulated
38809	SP_1669, SP_1670	2/3	Upregulated
38833	SP_1774, SP_1775	2/3	Upregulated
38839	SP_1802, SP_1803, SP_1804	3/4	Upregulated
38854	SP_1860, SP_1861, SP_1862, SP_1863	4/4	Upregulated
38857	SP_1869, SP_1870, SP_1871	3/3	Upregulated
38862	SP_1906, SP_1907	2/2	Upregulated
38884	SP_2001, SP_2002	2/6	Upregulated
38896	SP_2070, SP_2071	2/3	Upregulated
38917	SP_2174, SP_2175, SP_2176	3/5	Upregulated
38922	SP_2196, SP_2197	2/4	Upregulated
38930	SP_2239, SP_2240	2/2	Upregulated
38468	SP_0021, SP_0022	2/2	Downregulated
38469	SP_0024, SP_0025, SP_0026	3/3	Downregulated
38472	SP_0042, SP_0043	2/2	Downregulated
38476	SP_0053, SP_0054, SP_0055	3/4	Downregulated
38486	SP_0119, SP_0120	2/2	Downregulated
38495	SP_0151, SP_0152	2/3	Downregulated
38498	SP_0164, SP_0165	2/2	Downregulated
38510	SP_0220, SP_0221, SP_0222	3/14	Downregulated
38529	SP_0321, SP_0322, SP_0323, SP_0324, SP_0325, SP_0326	6/6	Downregulated
38533	SP_0352, SP_0354	2/9	Downregulated
38546	SP_0412, SP_0413	2/2	Downregulated

(*continued on next page*)

Table 1 (*continued*)

ID Operon	Locus	Expressed genes	Change
38547	SP_0416, SP_0417	2/2	Downregulated
38533	SP_0352, SP_0354	2/9	Downregulated
38546	SP_0412, SP_0413	2/2	Downregulated
38547	SP_0416, SP_0417	2/2	Downregulated
38548	SP_0419, SP_0420, SP_0421, SP_0422, SP_0423, SP_0424, SP_0425, SP_0426, SP_0427, SP_0428, SP_0429, SP_0430, SP_0431	13/13	Downregulated
38571	SP_0526, SP_0527	2/3	Downregulated
38610	SP_0701, SP_0702	2/2	Downregulated
38617	SP_0737, SP_0738	2/2	Downregulated
38620	SP_0750, SP_0751, SP_0752, SP_0753	4/4	Downregulated
38624	SP_0768, SP_0770	2/4	Downregulated
38627	SP_0785, SP_0786, SP_0787	3/3	Downregulated
38655	SP_0918, SP_0919, SP_0920, SP_0921, SP_0922	5/5	Downregulated
38665	SP_0963, SP_0964	2/2	Downregulated
38674	SP_1013, SP_1014	2/2	Downregulated
38682	SP_1069, SP_1070, SP_1071	3/6	Downregulated
38684	SP_1079, SP_1080	2/2	Downregulated
38726	SP_1276, SP_1277, SP_1278	3/3	Downregulated
38731	SP_1294, SP_1295	2/3	Downregulated
38751	SP_1402, SP_1404, SP_1405	3/4	Downregulated
38757	SP_1428, SP_1429	2/2	Downregulated
38763	SP_1460, SP_1461	2/2	Downregulated
38764	SP_1462, SP_1463, SP_1464	3/3	Downregulated
38765	SP_1465, SP_1466	2/2	Downregulated
38778	SP_1522, SP_1523	2/7	Downregulated
38815	SP_1686, SP_1687, SP_1688, SP_1689	4/4	Downregulated
38822	SP_1724, SP_1725	2/2	Downregulated
38840	SP_1809, SP_1810	2/2	Downregulated
38867	SP_1920, SP_1922	2/3	Downregulated
38868	SP_1923, SP_1924, SP_1925, SP_1926	4/4	Downregulated
38873	SP_1948, SP_1949	2/2	Downregulated
38874	SP_1951, SP_1952, SP_1953, SP_1954	4/5	Downregulated
38898	SP_2085, SP_2086, SP_2087, SP_2088	4/4	Downregulated
38906	SP_2115, SP_2117	2/3	Downregulated
38907	SP_2118, SP_2119	2/3	Downregulated
38929	SP_2235, SP_2236	2/3	Downregulated

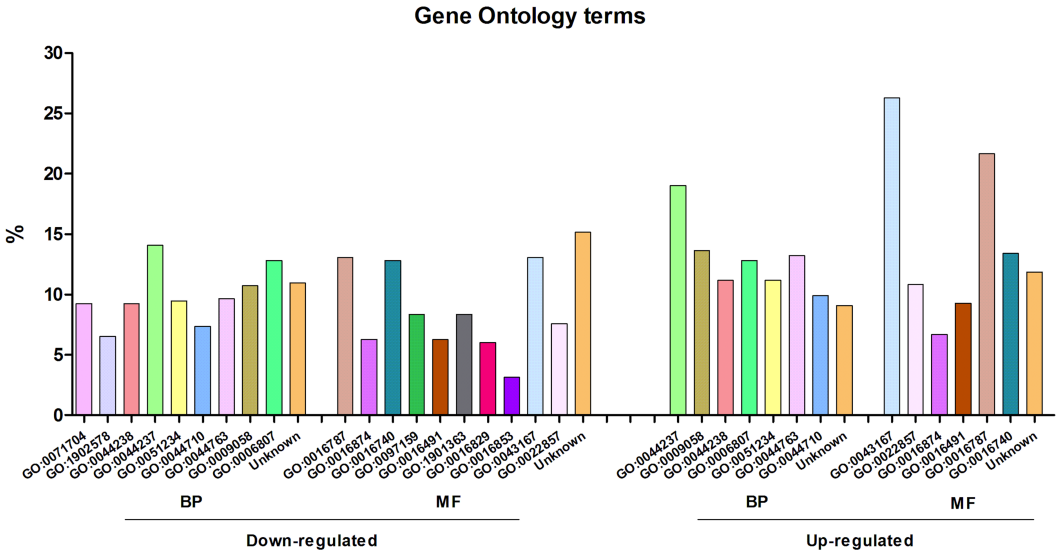

Figure 2 Gene Ontology analysis of the differentially expressed genes of *Streptococcus pneumoniae* TIGR4 after deferoxamine treatment. Gene Ontology terms were retrieved from annotated genes or their orthologs in case of non-annotated genes using BLAST2GO. Terms are indicated in the GO nomenclature. BP, biological process; MF, molecular function.

Full-size DOI: 10.7717/peerj.4966/fig-2

qualitative (i.e., absolute appearance or disappearance of a protein in a condition compared to the other one) and quantitative changes (i.e., changes in protein abundance on spots present in both conditions) when comparing for each protein fraction the iron starvation condition with its non-iron deprived control (Tables 2 and 3).

For the two analyzed protein fractions, most of the changes corresponded to predicted cytoplasmic proteins, mainly affecting enzymes of the primary metabolism. Glyceraldehyde-3-phosphate dehydrogenase was less abundant under iron deprivation. This enzyme was strongly reduced in total extracts after DFO treatment (fold-change decrease > 4), as well as not detected in the secretome fraction of DFO-exposed culture (but detected in the control secretome). Another enzyme of the glycolysis pathway that also decreased its abundance was the phosphoglycerate kinase. Other two Mg^{2+}-dependent enzymes of the glycolysis pathway, enolase and pyruvate kinase, also decreased in secretomes of DFO-exposed cells. We also found that one enzyme of the fatty acid biosynthesis pathway was more abundant under iron deprivation: 3-oxoacyl-[acyl-carrier protein] reductase in total extracts (fold change around 7). Also, two major and very abundant extracellular proteins were detected to decrease in DFO-treated cultures: the choline-binding protein A (SP_2190) and the PcsB protein (SP_2216).

We also found a decrease in the abundance levels of an enzyme taking part in the recycling pathway of amino sugar compounds: the divalent cation-dependent *N*-acetylglucosamine-6-phosphate deacetylase, SP_2056 (NagA), which was found to be almost ninefold less abundant in DFO-exposed secretomes.

Other cation-containing or dependent enzymes decreased their abundances under iron deprivation conditions. Thus, lower levels of zinc-containing alcohol dehydrogenase

Table 2 **Protein identification by MALDI-TOF/TOF of qualitative changes in the protein abundances of *Streptococcus pneumoniae* TIGR4 after deferoxamine treatment.**

Spot	Abundance	Locus	Protein name	Score[a]	Location[b]
TE1	Decreased	SP_1284	LemA protein	300	Membrane
TE2	Decreased	SP_1271	2-C-methyl-D-erythritol 4-phosphate cytidylyltransferase	349	Cytoplasmic
TE3	Increased	SP_0845	Basic membrane family protein	942	Extracellular
TE4	Increased	SP_1362	Glutamate dehydrogenase	837	Cytoplasmic
TS1	Decreased	SP_1004	Uncharacterized protein	410	Extracellular
TS2	Decreased	SP_0341	UPF0371 protein SP_0341	877	Cytoplasmic
TS3	Decreased	SP_0012	Hypoxanthine-guanine phosphoribosyl-transferase	749	Cytoplasmic
TS4	Decreased	SP_1229	Formate–tetrahydrofolate ligase	650	Cytoplasmic
TS5	Decreased	SP_0027	Ribose-phosphate pyrophosphokinase 1	665	Cytoplasmic
TS6	Decreased	SP_0746	ATP-dependent Clp protease proteolytic subunit	81	Cytoplasmic
TS7	Decreased	SP_2190	Choline binding protein A	174	Extracellular
TS8	Decreased	SP_0715	Lactate oxidase	686	Cytoplasmic
TS9	Decreased	SP_2216	Secreted 45 kd protein	512	Extracellular
TS10	Decreased	SP_1456	Peptide deformylase (PDF)	251	Cytoplasmic
TS11	Decreased	SP_0459	Formate acetyltransferase	152	Cytoplasmic
TS12	Decreased	SP_1534	Probable manganese-dependent inorganic pyrophosphatase	533	Cytoplasmic
TS13	Decreased	SP_0516	Protein GrpE (HSP-70 cofactor)	178	Cytoplasmic
TS14	Decreased	SP_2012	Glyceraldehyde-3-phosphate dehydrogenase	451	Cytoplasmic
TS15	Decreased	SP_1445	GMP synthase [glutamine-hydrolyzing]	676	Cytoplasmic
TS16	Decreased	SP_0236	DNA-directed RNA polymerase subunit alpha (RNAP subunit alpha)	152	Cytoplasmic
TS17	Decreased	SP_1922	Probable transcriptional regulatory protein SP_1922	418	Cytoplasmic
TS18	Decreased	SP_0435	Elongation factor P (EF-P)	290	Cytoplasmic
TS19	Decreased	SP_2084	Phosphate-binding protein PstS 2 (PBP 2)	862	Extracellular
TS20	Decreased	SP_1999	Catabolite control protein A	937	Cytoplasmic
TS21	Decreased	SP_1508	ATP synthase subunit beta	261	Cytoplasmic
TS22	Decreased	SP_0745	Uracil phosphoribosyltransferase	702	Cytoplasmic
TS23	Increased	SP_0862	Ribosomal protein S3	424	Cytoplasmic

Notes.

[a]Mascot scores >70 were considered significant at $p < 0.05$.

[b]Protein localization in subcellular compartments was assigned using LocateP.

and manganese-dependent inorganic pyrophosphatase were detected, as well as of hypoxanthine-guanine phosphoribosyltransferase, which requires Mg^{2+} as a cofactor.

Metabolomics

Finally, we studied the changes in the metabolic profile of intracellular metabolite fractions from both pneumococcal strains, by using LC–MS/MS, which allowed detection of 719 and

Table 3 **Protein identification by MALDI-TOF/TOF of quantitative changes (>2 fold change (FC)) in the protein abundances of *Streptococcus pneumoniae* TIGR4 after deferoxamine treatment.**

Spot	Abundance	FC[a]	*p*-value	Locus	Protein name	Score[b]	Location[c]
TE5	Increased	6.1	0.03	SP_1220	L-lactate dehydrogenase	607	Cytoplasmic
TE6	Increased	6.9	0.01	SP_0421	3-oxoacyl-[acyl-carrier protein] reductase	528	Cytoplasmic
TE7	Decreased	4.6	0.04	SP_2055	Alcohol dehydrogenase, zinc-containing	535	Cytoplasmic
TE8	Decreased	4.3	0.03	SP_2012	Glyceraldehyde-3-phosphate dehydrogenase	255	Cytoplasmic
TS24	Increased	4.4	0.02	nanA	Sialidase A	185	Cell wall
TS25	Decreased	4.2	0.02	SP_0499	phosphoglycerate kinase	991	Cytoplasmic
TS26	Decreased	4.5	0.04	SP_1489	Elongation factor Tu	1,120	Cytoplasmic
TS27	Decreased	6.6	0.03	SP_0897	Pyruvate kinase	708	Cytoplasmic
TS28	Decreased	8.8	0.01	SP_2056	N-acetylglucosamine-6-phosphate deacetylase	587	Cytoplasmic
TS29	Decreased	4.2	0.03	SP_1128	Enolase	349	Cytoplasmic
TS30	Decreased	4.1	0.04	SP_1541	30S ribosomal protein S6	114	Cytoplasmic
TS31	Decreased	4.4	0.04	SP_1910	Uncharacterized protein	523	Cytoplasmic

Notes.

[a]For increased proteins, the FC was calculated as the treatment/control ratio; for decreased proteins, the FC was calculated as the control/treatment ratio.

[b]Mascot scores >70 were considered significant at $p < 0.05$.

[c]Protein localization in subcellular compartments was assigned using LocateP.

826 different chromatographic peaks, in negative and positive ionization mode, respectively. Statistical analysis by Volcano plot revealed that 64 entities presented a *p*-value below 0.05 and a fold change, in terms of relative concentrations, higher than 2 for discrimination between treated and non-treated TIGR4 samples (data not shown).

A multivariate statistical analysis was carried out with significant entities to evaluate whether the iron deprivation treatment had an effect on the metabolite profile. Figure S5 shows the principal component analysis (PCA) of identified metabolites when comparing iron-depleted and non-depleted cultures, revealing that the first principal component (*X*-axis) clearly grouped the three control biological replicates, which were clearly separated from two out of the three DFO-treated samples. However, there was dispersion in the three biological replicates of the DFO treatment, as the first principal component did not group them.

The tentative identification of significantly changing entities led to a panel of 17 compounds (Table 4). Although the number of changing metabolites positively identified was low, we clearly found an increase in the concentration of intermediate amino sugar metabolites involved in the cell wall peptidoglycan metabolism: there was an increase in uridine-5′-diphosphoglucuronic acid (2.2-fold), UDP-*N*-acetylmuraminate (>20-fold), *N*-acetylglucosamine (3.8-fold), and UDP-*N*-acetylglucosamine (2.4-fold).

DISCUSSION

There is little knowledge about the mechanisms of iron intake by the pneumococcus (*Hoyer et al., in press*). In this work, we have approached a multi-omics strategy to understand the changes at the molecular level occurring in the pneumococcus during iron deprivation, similarly to what theoretically happens during an *in vivo* infection. To our knowledge, this is a unique study carried out so far for iron deprivation in this human pathogen using

Table 4 Metabolites altered after deferoxamine treatment of *Streptococcus pneumoniae* TIGR4.

Metabolite	Retention time (min)	Abundance	Fold change[a]	*p*-value
C-di-AMP	5.86	Increased	3.9	0.02
Uridine-5′-diphosphoglucuronic acid	6.22	Increased	2.2	0.03
UDP-N-acetylmuraminate	1.50	Increased	20.2	0.01
UDP-N-acetylglucosamine	2.02	Increased	2.4	0.04
cAMP	5.94	Increased	3.4	0.03
Tri-N-acetylchitotriose	6.04	Increased	2.3	0.03
Purine	2.37	Increased	10.1	0.01
dTMP	5.98	Decreased	12.6	0.01
Adenosine 5-monophosphate	5.80	Decreased	17.9	0.01
GDP-glucose	6.44	Decreased	2.5	0.04
GDP	3.04	Decreased	2.1	0.03
deoxyAMP	5.06	Decreased	10.5	0.01
Guanine	5.96	Decreased	8.5	0.01
deoxyGMP	5.88	Decreased	12.0	0.01
GluMet	6.16	Decreased	2.4	0.03
Metionine	6.16	Decreased	2.4	0.02
N-acetylglucosamine	6.29	Decreased	3.8	0.02

Notes.

[a]For increased metabolites, the FC was calculated as the treatment/control ratio; for decreased metabolites, the FC was calculated as the control/treatment ratio.

three different "omics". Very recently, a combined translatomics/proteomics approach has been applied to identify novel iron-transporting proteins in the pneumococcus (*Yang et al., 2016*). Previously, it had been approached using only proteomics (*Nanduri et al., 2008*; *Yang et al., 2015*).

We selected as iron chelator the DFO, which has been described to have high iron chelating specificity, although it might also sequester other divalent cations (*Eichenbaum, Green & Scott, 1996*). We chose the culture points at which almost no alterations in growth were observed, as described for other studies in bacteria in which this iron chelator was used at the same or very similar concentration (*Basler et al., 2006*; *Smith et al., 2001*; *Trappetti et al., 2011*). These conditions were applied to obtain transcriptome, proteome and metabolome preparations of the reference pneumococcal strain TIGR4.

Our transcriptomic analysis showed very consistent and reproducible results between biological replicates. The range of $\log_2$ fold changes was apparently low, ranging between 1.78 and −2.13, but the numbers obtained were in general quite similar to those observed for transcriptomic analyses of iron starvation in other microorganisms (*Allen et al., 2010*; *Basler et al., 2006*; *Brickman et al., 2011*; *Klitgaard et al., 2010*; *Madsen et al., 2006*). However, very interestingly the changes observed in our work were in most cases for genes grouped in operons, and genes belonging to the same operon underwent, as expected, almost identical fold change values. This is another argument that confirms the validity of our microarray results, as already described in similar works (*Allen et al., 2010*; *Klitgaard et al., 2010*; *Vasileva et al., 2012*).

In TIGR4, we found an up-regulation of 29 operons, and a down-regulation of 44 operons. Among those being over-expressed, we found two operons coding for iron-compound ABC transport systems, both of them localized together in the genome: the operon 38857 (genes SP_1869 to SP_1871) and the operon 1446903 (containing only one gene, SP_1872). The TIGR4 genome has other operon (no. 38677) containing four genes (SP_1032 to SP_1035) participating in a third iron-compound ABC system, but this operon was not found differentially expressed in our study. The up-regulation of the manganese ABC transporter system (operon 38805) could indicate that the chelator used is not completely specific for iron, as already known, but it cannot be ruled out that this operon might have a function related to iron uptake. Actually, recently *Yang et al. (2016)* have reported the over-expression in the *S. pneumoniae* D39 strain of genes coding for sugar and other substrate-ABC transporters and validated one of them at the protein level, thus indicating that iron deprivation may affect other transporter systems which are not annotated in databases as "iron transporters". We also found the up-regulation of the operon 38501, responsible for riboflavin biosynthesis. Very recently, it has been described in *Vibrio cholerae* the cross-modulatory effect between riboflavin and iron (*Sepulveda-Cisternas et al., 2018*). Among the down-expressed operons, we found some transporter systems, as the branched-chain amino acid ABC transporter system (operon 38620, genes SP_0750 to SP_0753), a fluoride ion transporter system (genes SP_1294 and SP_1295) or a phosphate ABC transporter system (genes SP_2085 to SP_2088). We ignore the meaning of these changes, but this work opens new possibilities to explore the role of these genes in the iron uptake.

In previous works, we have analyzed the surface proteome ("surfome") of the pneumococcus specifically targeting the discovery of vaccine or diagnostic candidates (*Jimenez-Munguia et al., 2015*; *Olaya-Abril et al., 2012*; *Olaya-Abril et al., 2013*; *Olaya-Abril et al., 2015*). In this study, we searched for proteome changes using 2-D gel-based analysis on total cell extract and secretome fractions. As expected, most changes were in cytoplasmic proteins, as these are the most abundant ones in the bacterial cells. This class of proteins was also found in the secretome fractions, as extensively reported for numerous works in a wide variety of microorganisms (for an extensive review about the presence and role of cytoplasmic proteins in extracellular and/or surface protein preparations, see *Olaya-Abril et al., 2014a*).

Many of the changes observed in our work are coinciding with other results already described in the pneumococcus and other microorganisms. In the present study, the enzyme GAPDH was less abundant in iron-depleted protein fractions, as reported for pneumococcus (*Nanduri et al., 2008*) and *Staphylococcus aureus* (*Friedman et al., 2006*). This protein has been described as a moonlighting protein with different functions, including an important role in iron metabolism (*Boradia, Raje & Raje, 2014*). The zinc-containing alcohol dehydrogenase has been also described to be less abundant in iron-depleted *S. aureus* protein fractions (*Friedman et al., 2006*). We found a decrease in some Mg^{2+}-dependent glycolytic enzymes (phosphoglycerate kinase, enolase, pyruvate kinase), which might be due to the partially non-specific sequestration of this cation by DFO. Very

similar results have been obtained in pneumococcal biofilms, where iron is less available than in planktonic cultures (*Allan et al., 2014*; *Trappetti et al., 2011*).

In a very recent paper, Hoyer and colleagues have studied the changes in the proteome of *Streptococcus pneumoniae* D39 under iron deprivation using 2,2′-bipyridine as chelator, in two different culture media (*Hoyer et al., in press*). They have performed the proteomic analysis by LC-MS/MS, which is much more sensitive than our 2-DE/MALDI-TOF approach for detecting both high numbers of proteins and changes in their abundances. However, in spite of using different strains, growth media and proteomic approaches, by comparing our results with those obtained in the THY medium in this cited work, there is a strong coincidence in the protein changes: 16 out of our 38 changing different proteins (namely SP_1284, SP_2190, SP_1456, SP_0459, 1534, SP_2012, SP_0236, SP_1508, SP_0421, SP_2055, SP_0499, SP_1489, SP_0897, SP_2056, and SP_1128) changed accordingly in both works. Many of the proteins are cation-dependent, as already described above. Interestingly, one of the common changes is the NagA.

Perhaps metabolomics data are generally the most difficult ones to integrate with the other "omes", as it is still a step backwards compared to transcriptomics and proteomics. There are very few studies on metabolomics in bacteria. We have recently published a work of proteomics and metabolomics integration in the pneumococcus to study the effect of an antimicrobial compound (*Mitsuwan et al., 2017*). Very recently, Leonard and colleagues have described the metabolome inventory of a non-encapsulated *S. pneumoniae* TIGR4 in a chemically-defined medium, and using three techniques: ^{1}H-NMR, HPLC-MS and GC-MS (*Leonard et al., in press*). Although these results are not comparable to ours (different growth medium, different methods and purpose), the cited work reveals the identification of some tens of metabolites, with a predominance of precursors of peptidoglycan synthesis (UDP-MurNAc, UDP-GlcNAc) as in our study. In this present work, we unambiguously detected only a few compounds changing after DFO treatment. Partially, this could be due to the variability in the three DFO-treated metabolome samples, as observed in Fig. S5. In addition, we could not calculate the adenylate energy charge, a well accepted quality control in metabolomic preparations, as we did not unambiguously identify ATP in our samples. These two issues indicate that our metabolomic data should be interpreted with caution. Nevertheless, some of the changes detected were in metabolites related to peptidoglycan metabolism. Very interestingly, the enzyme NagA, taking part in the amino sugar metabolism, was clearly depleted. Actually, according to the UniProtKB database, NagA has divalent cations as cofactors, including Fe^{2+}, as it possesses a conserved domain belonging to the metallo-dependent hydrolases superfamily. NagA deacetylates GlcNAc-6P to GlcN-6P. The increase observed in our work in GlcNAc, a precursor of GlcNAc-6P, might be due to the decrease in enzymes like NagA that avoid their by-products conversions. This protein has been recently detected in the pneumococcal secreted fraction as in our work, and has been proposed as a pneumococcal diagnostic marker because of its high immunogenicity (*Choi et al., 2013*).

In our opinion this work shows a possible unknown effect of iron deprivation on the global physiology of the bacterium, as it seems to be a relationship among iron starvation, the depletion of this enzyme and the alteration of the above discussed metabolites. Further

research will be needed to go in depth in this aspect. This may help to identify pathways or biomolecules that can be used as targets for therapies against pneumococcal infection.

CONCLUSIONS

A global multi-omic analysis has been carried out to study the effect of iron limitation in the pneumococcus, similarly to what occurs during in vivo infection within the host. A significant number of genes changed in their expression, many of them involved in ion binding functions. Proteomics revealed changes in enzymes participating in the primary and peptidoglycan metabolism, many of them being cation-dependent. The metabolomic analysis revealed some changes in the levels of intermediates involved in the peptidoglycan biosynthesis. The different "omics" show sets of changing biomolecules that can complement themselves to provide a global insight into the adaptation of pneumococcus to iron starvation.

ACKNOWLEDGEMENTS

MALDI-TOF/TOF and ICP-MS analyses were performed at the Proteomics and the Mass Spectrometry Facilities, respectively (SCAI, University of Córdoba). We are indebted to members of the AGR-164 group, University of Córdoba, for lab support.

ADDITIONAL INFORMATION AND DECLARATIONS

Funding

This research was funded by Project Grants FIS-P12/01259 (Spanish Ministry of Economy and Competitiveness), P09-CTS-4616 from Consejería de Innovación, Ciencia y Empresa (Junta de Andalucía), to Manuel José Rodríguez-Ortega, and by FEDER funds from the EU. The funders had no role in study design, data collection and analysis, decision to publish, or preparation of the manuscript.

Grant Disclosures

The following grant information was disclosed by the authors:
Spanish Ministry of Economy and Competitiveness: FIS-P12/01259.
Consejería de Innovación, Ciencia y Empresa: P09-CTS-4616.
FEDER.

Competing Interests

The authors declare there are no competing interests.

Author Contributions

- Irene Jiménez-Munguía conceived and designed the experiments, performed the experiments, analyzed the data, prepared figures and/or tables, authored or reviewed drafts of the paper, approved the final draft.
- Mónica Calderón-Santiago performed the experiments, authored or reviewed drafts of the paper, approved the final draft.

- Antonio Rodríguez-Franco analyzed the data, contributed reagents/materials/analysis tools, prepared figures and/or tables, authored or reviewed drafts of the paper, approved the final draft.
- Feliciano Priego-Capote analyzed the data, contributed reagents/materials/analysis tools, authored or reviewed drafts of the paper, approved the final draft.
- Manuel J. Rodríguez-Ortega conceived and designed the experiments, analyzed the data, contributed reagents/materials/analysis tools, prepared figures and/or tables, authored or reviewed drafts of the paper, approved the final draft.

Data Availability

The following information was supplied regarding data availability:

The complete design of the microarray was deposited at the Gene Expression Omnibus NCBI database, with accession number GSE109693 (https://www.ncbi.nlm.nih.gov/geo/query/acc.cgi?acc=GSE109693).

Supplemental Information

Supplemental information for this article can be found online at http://dx.doi.org/10.7717/peerj.4966#supplemental-information.

REFERENCES

Allan RN, Skipp P, Jefferies J, Clarke SC, Faust SN, Hall-Stoodley L, Webb J. 2014. Pronounced metabolic changes in adaptation to biofilm growth by *Streptococcus pneumoniae*. *PLOS ONE* **9**:e107015 DOI 10.1371/journal.pone.0107015.

Allen KJ, Lepp D, McKellar RC, Griffiths MW. 2010. Targeted microarray analysis of stationary phase Escherichia coli O157:H7 subjected to disparate nutrient conditions. *Journal of Applied Microbiology* **109**:2118–2127 DOI 10.1111/j.1365-2672.2010.04843.x.

Basler M, Linhartova I, Halada P, Novotna J, Bezouskova S, Osicka R, Weiser J, Vohradsky J, Sebo P. 2006. The iron-regulated transcriptome and proteome of Neisseria meningitidis serogroup C. *Proteomics* **6**:6194–6206 DOI 10.1002/pmic.200600312.

Blasi F, Mantero M, Santus P, Tarsia P. 2012. Understanding the burden of pneumococcal disease in adults. *Clinical Microbiology and Infection* **18(Suppl 5)**:7–14 DOI 10.1111/j.1469-0691.2012.03937.x.

Boradia VM, Raje M, Raje CI. 2014. Protein moonlighting in iron metabolism: glyceraldehyde-3-phosphate dehydrogenase (GAPDH). *Biochemical Society Transactions* **42**:1796–1801 DOI 10.1042/BST20140220.

Bradford MM. 1976. A rapid and sensitive method for the quantitation of microgram quantities of protein utilizing the principle of protein-dye binding. *Analytical Biochemistry* **72**:248–254 DOI 10.1016/0003-2697(76)90527-3.

Brickman TJ, Cummings CA, Liew SY, Relman DA, Armstrong SK. 2011. Transcriptional profiling of the iron starvation response in Bordetella pertussis provides

new insights into siderophore utilization and virulence gene expression. *Journal of Bacteriology* **193**:4798–4812 DOI 10.1128/JB.05136-11.

Choi CW, An HY, Lee YJ, Lee YG, Yun SH, Park EC, Hong Y, Kim GH, Park JE, Baek SJ, Kim HS, Kim SI. 2013. Characterization of Streptococcus pneumoniae N-acetylglucosamine-6-phosphate deacetylase as a novel diagnostic marker. *Journal of Microbiology* **51**:659–664 DOI 10.1007/s12275-013-3451-8.

Conesa A, Gotz S, Garcia-Gomez JM, Terol J, Talon M, Robles M. 2005. Blast2GO: a universal tool for annotation, visualization and analysis in functional genomics research. *Bioinformatics* **21**:3674–3676 DOI 10.1093/bioinformatics/bti610.

Dall'Agnol HP, Barauna RA, De Sa PH, Ramos RT, Nobrega F, Nunes CI, Das Gracas DA, Carneiro AR, Santos DM, Pimenta AM, Carepo MS, Azevedo V, Pellizari VH, Schneider MP, Silva A. 2014. Omics profiles used to evaluate the gene expression of Exiguobacterium antarcticum B7 during cold adaptation. *BMC Genomics* **15**:986 DOI 10.1186/1471-2164-15-986.

Dam P, Olman V, Harris K, Su Z, Xu Y. 2007. Operon prediction using both genome-specific and general genomic information. *Nucleic Acids Research* **35**:288–298 DOI 10.1093/nar/gkl1018.

Eichenbaum Z, Green BD, Scott JR. 1996. Iron starvation causes release from the group A streptococcus of the ADP-ribosylating protein called plasmin receptor or surface glyceraldehyde-3-phosphate-dehydrogenase. *Infection and Immunity* **64**:1956–1960.

Feng J, Billal DS, Lupien A, Racine G, Winstall E, Legare D, Leprohon P, Ouellette M. 2011. Proteomic and transcriptomic analysis of linezolid resistance in Streptococcus pneumoniae. *Journal of Proteome Research* **10**:4439–4452 DOI 10.1021/pr200221s.

Fondi M, Lio P. 2015. Multi -omics and metabolic modelling pipelines: challenges and tools for systems microbiology. *Microbiological Research* **171**:52–64 DOI 10.1016/j.micres.2015.01.003.

Friedman DB, Stauff DL, Pishchany G, Whitwell CW, Torres VJ, Skaar EP. 2006. Staphylococcus aureus redirects central metabolism to increase iron availability. *PLOS Pathogens* **2**:e87 DOI 10.1371/journal.ppat.0020087.

Froehlich BJ, Bates C, Scott JR. 2009. Streptococcus pyogenes CovRS mediates growth in iron starvation and in the presence of the human cationic antimicrobial peptide LL-37. *Journal of Bacteriology* **191**:673–677 DOI 10.1128/JB.01256-08.

Fu F, Cheng VW, Wu Y, Tang Y, Weiner JH, Li L. 2013. Comparative proteomic and metabolomic analysis of Staphylococcus warneri SG1 cultured in the presence and absence of butanol. *Journal of Proteome Research* **12**:4478–4489 DOI 10.1021/pr400533m.

Ge R, Sun X. 2014. Iron acquisition and regulation systems in Streptococcus species. *Metallomics* **6**:996–1003 DOI 10.1039/c4mt00011k.

Grady SL, Malfatti SA, Gunasekera TS, Dalley BK, Lyman MG, Striebich RC, Mayhew MB, Zhou CL, Ruiz ON, Dugan LC. 2017. A comprehensive multi-omics approach uncovers adaptations for growth and survival of Pseudomonas aeruginosa on n-alkanes. *BMC Genomics* **18**:334 DOI 10.1186/s12864-017-3708-4.

Hoyer J, Bartel J, Gomez-Mejia A, Rohde M, Hirschfeld C, Hess N, Sura T, Maass S, Hammerschmidt S, Becher D. 2018. Proteomic response of Streptococcus pneumoniae to iron limitation. *International Journal of Medical Microbiology* In Press DOI 10.1016/j.ijmm.2018.02.001.

Jimenez-Munguia I, Van Wamel WJ, Olaya-Abril A, Garcia-Cabrera E, Rodriguez-Ortega MJ, Obando I. 2015. Proteomics-driven design of a multiplex bead-based platform to assess natural IgG antibodies to pneumococcal protein antigens in children. *Journal of Proteomics* **126**:228–233 DOI 10.1016/j.jprot.2015.06.011.

Johnson HL, Deloria-Knoll M, Levine OS, Stoszek SK, Freimanis Hance L, Reithinger R, Muenz LR, O'Brien KL. 2010. Systematic evaluation of serotypes causing invasive pneumococcal disease among children under five: the pneumococcal global serotype project. *PLOS Medicine* **7**:e1000348 DOI 10.1371/journal.pmed.1000348.

Kanaujia PK, Bajaj P, Kumar S, Singhal N, Virdi JS. 2015. Proteomic analysis of Yersinia enterocolitica biovar 1A under iron-rich and iron-poor conditions indicate existence of efficiently regulated mechanisms of iron homeostasis. *Journal of Proteomics* **124**:39–49 DOI 10.1016/j.jprot.2015.04.015.

Klitgaard K, Friis C, Angen O, Boye M. 2010. Comparative profiling of the transcriptional response to iron restriction in six serotypes of Actinobacillus pleuropneumoniae with different virulence potential. *BMC Genomics* **11**:698 DOI 10.1186/1471-2164-11-698.

Kohlstedt M, Sappa PK, Meyer H, Maass S, Zaprasis A, Hoffmann T, Becker J, Steil L, Hecker M, Van Dijl JM, Lalk M, Mader U, Stulke J, Bremer E, Volker U, Wittmann C. 2014. Adaptation of Bacillus subtilis carbon core metabolism to simultaneous nutrient limitation and osmotic challenge: a multi-omics perspective. *Environmental Microbiology* **16**:1898–1917 DOI 10.1111/1462-2920.12438.

Leonard A, Gierok P, Methling K, Gomez-Mejia A, Hammerschmidt S, Lalk M. 2018. Metabolic inventory of Streptococcus pneumoniae growing in a chemical defined environment. *International Journal of Medical Microbiology* S1438–S4221 In Press DOI 10.1016/j.ijmm.2018.01.001.

Madsen ML, Nettleton D, Thacker EL, Minion FC. 2006. Transcriptional profiling of Mycoplasma hyopneumoniae during iron depletion using microarrays. *Microbiology* **152**:937–944 DOI 10.1099/mic.0.28674-0.

Mao F, Dam P, Chou J, Olman V, Xu Y. 2009. DOOR: a database for prokaryotic operons. *Nucleic Acids Research* **37**:D459–D463 DOI 10.1093/nar/gkn757.

Mitsuwan W, Olaya-Abril A, Calderon-Santiago M, Jimenez-Munguia I, Gonzalez-Reyes JA, Priego-Capote F, Voravuthikunchai SP, Rodriguez-Ortega MJ. 2017. Integrated proteomic and metabolomic analysis reveals that rhodomyrtone reduces the capsule in Streptococcus pneumoniae. *Scientific Reports* **7**:2715 DOI 10.1038/s41598-017-02996-3.

Nanduri B, Shah P, Ramkumar M, Allen EB, Swiatlo E, Burgess SC, Lawrence ML. 2008. Quantitative analysis of Streptococcus pneumoniae TIGR4 response to *in vitro* iron restriction by 2-D LC ESI MS/MS. *Proteomics* **8**:2104–2114 DOI 10.1002/pmic.200701048.

O'Brien KL, Wolfson LJ, Watt JP, Henkle E, Deloria-Knoll M, McCall N, Lee E, Mulholland K, Levine OS, Cherian T, Hib and Pneumococcal Global Burden of Disease Study Team. 2009. Burden of disease caused by Streptococcus pneumoniae in children younger than 5 years: global estimates. *Lancet* **374**:893–902 DOI 10.1016/S0140-6736(09)61204-6.

Olaya-Abril A, Gomez-Gascon L, Jimenez-Munguia I, Obando I, Rodriguez-Ortega MJ. 2012. Another turn of the screw in shaving Gram-positive bacteria: optimization of proteomics surface protein identification in Streptococcus pneumoniae. *Journal of Proteomics* **75**:3733–3746 DOI 10.1016/j.jprot.2012.04.037.

Olaya-Abril A, Jimenez-Munguia I, Gomez-Gascon L, Obando I, Rodriguez-Ortega MJ. 2013. Identification of potential new protein vaccine candidates through pan-surfomic analysis of pneumococcal clinical isolates from adults. *PLOS ONE* **8**:e70365 DOI 10.1371/journal.pone.0070365.

Olaya-Abril A, Jimenez-Munguia I, Gomez-Gascon L, Obando I, Rodriguez-Ortega MJ. 2015. A pneumococcal protein array as a platform to discover serodiagnostic antigens against infection. *Molecular & Cellular Proteomics* **14**:2591–2608 DOI 10.1074/mcp.M115.049544.

Olaya-Abril A, Jimenez-Munguia I, Gomez-Gascon L, Rodriguez-Ortega MJ. 2014a. Surfomics: shaving live organisms for a fast proteomic identification of surface proteins. *Journal of Proteomics* **97**:164–176 DOI 10.1016/j.jprot.2013.03.035.

Olaya-Abril A, Prados-Rosales R, McConnell MJ, Martin-Pena R, Gonzalez-Reyes JA, Jimenez-Munguia I, Gomez-Gascon L, Fernandez J, Luque-Garcia JL, Garcia-Lidon C, Estevez H, Pachon J, Obando I, Casadevall A, Pirofski LA, Rodriguez-Ortega MJ. 2014b. Characterization of protective extracellular membrane-derived vesicles produced by Streptococcus pneumoniae. *Journal of Proteomics* **106**:46–60 DOI 10.1016/j.jprot.2014.04.023.

Ritchie ME, Phipson B, Wu D, Hu Y, Law CW, Shi W, Smyth GK. 2015. limma powers differential expression analyses for RNA-sequencing and microarray studies. *Nucleic Acids Research* **43**:e47 DOI 10.1093/nar/gkv007.

Sepulveda-Cisternas I, Lozano Aguirre L, Fuentes Flores A, Vasquez Solis de Ovando I, Garcia-Angulo VA. 2018. Transcriptomics reveals a cross-modulatory effect between riboflavin and iron and outlines responses to riboflavin biosynthesis and uptake in Vibrio cholerae. *Scientific Reports* **8**:3149 DOI 10.1038/s41598-018-21302-3.

Sharov AA, Dudekula DB, Ko MS. 2005. A web-based tool for principal component and significance analysis of microarray data. *Bioinformatics* **21**:2548–2549 DOI 10.1093/bioinformatics/bti343.

Smith HE, Buijs H, De Vries RR, Wisselink HJ, Stockhofe-Zurwieden N, Smits MA. 2001. Environmentally regulated genes of Streptococcus suis: identification by the use of iron-restricted conditions *in vitro* and by experimental infection of piglets. *Microbiology* **147**:271–280 DOI 10.1099/00221287-147-2-271.

Trappetti C, Potter AJ, Paton AW, Oggioni MR, Paton JC. 2011. LuxS mediates iron-dependent biofilm formation, competence, and fratricide in Streptococcus pneumoniae. *Infection and Immunity* **79**:4550–4558 DOI 10.1128/IAI.05644-11.

Vasileva D, Janssen H, Honicke D, Ehrenreich A, Bahl H. 2012. Effect of iron limitation and fur gene inactivation on the transcriptional profile of the strict anaerobe Clostridium acetobutylicum. *Microbiology* **158**:1918–1929 DOI 10.1099/mic.0.056978-0.

Weycker D, Strutton D, Edelsberg J, Sato R, Jackson LA. 2010. Clinical and economic burden of pneumococcal disease in older US adults. *Vaccine* **28**:4955–4960 DOI 10.1016/j.vaccine.2010.05.030.

Yang S, Giannone RJ, Dice L, Yang ZK, Engle NL, Tschaplinski TJ, Hettich RL, Brown SD. 2012. Clostridium thermocellum ATCC27405 transcriptomic, metabolomic and proteomic profiles after ethanol stress. *BMC Genomics* **13**:336 DOI 10.1186/1471-2164-13-336.

Yang XY, He K, Du G, Wu X, Yu G, Pan Y, Zhang G, Sun X, He QY. 2016. Integrated translatomics with proteomics to identify novel iron-transporting proteins in streptococcus pneumoniae. *Frontiers in Microbiology* **7**:78 DOI 10.3389/fmicb.2016.00078.

Yang XY, Sun B, Zhang L, Li N, Han J, Zhang J, Sun X, He QY. 2014. Chemical interference with iron transport systems to suppress bacterial growth of Streptococcus pneumoniae. *PLOS ONE* **9**:e105953 DOI 10.1371/journal.pone.0105953.

Yang XY, Zhang L, Liu J, Li N, Yu G, Cao K, Han J, Zeng G, Pan Y, Sun X, He QY. 2015. Proteomic analysis on the antibacterial activity of a Ru(II) complex against Streptococcus pneumoniae. *Journal of Proteomics* **115**:107–116 DOI 10.1016/j.jprot.2014.11.018.